

# Post-fault voltage limit assessment for six-phase induction machines: a synchronous and slip frequency approach

Nooradzianie Muhammad Zin<sup>1</sup>, Wan Noraishah Wan Abdul Munim<sup>1</sup>, Ahmad Farid Abidin<sup>2</sup>,  
Hang Seng Che<sup>3</sup>, Mohamad Fathi Mohamad Elias<sup>3</sup>, Rahimi Baharom<sup>1</sup>

<sup>1</sup>School of Electrical Engineering, College of Engineering, Universiti Teknologi MARA (UiTM), Shah Alam, Malaysia

<sup>2</sup>Centre of Foundation Studies, Universiti Teknologi MARA, Dengkil, Malaysia

<sup>3</sup>UM Power Energy Dedicated Advanced Center (UMPEDAC), University of Malaya, Kuala Lumpur, Malaysia

## Article Info

### Article history:

Received Jun 4, 2024

Revised Nov 20, 2024

Accepted Nov 28, 2024

### Keywords:

Current limit

Fault-tolerant capability

Six-phase machine

Slip frequency

Synchronous frequency

Voltage limit

## ABSTRACT

Six-phase machine research has attracted a lot of attention lately, as seen by the large number of articles and case studies that have been written about it. Six-phase induction machines are prevalent due to their simplicity in construction. A fault-tolerance system is essential to guaranteeing machine operation that is both available and continuous in the event of a disruption or failure in the system. The operational topologies of dual three-phase (D3-IM) and symmetrical six-phase (S6-IM) induction machines were studied in this research. One open-phase fault (1OPF) is covered in the study, and different scenarios including the derating factor, neutral configuration, and maximum torque (MT) operational strategy are taken into account. Using MATLAB software, machine characteristics, machine equations, and Clarke's transformation show the fault-tolerant capability of each type of machine. Moreover, a MATLAB program is developed to assess post-fault voltage control limits, allowing for a comparison between current and voltage control limits. Simulated graph results depicting line-to-line voltages against synchronous and slip frequencies across all possible fault scenarios reveal distinct fault-tolerant capabilities between the two machine types. The comparative study shows that S6-IM offers better fault-tolerant capability than D3-IM based on both various synchronous and slip frequencies approaches.

*This is an open access article under the [CC BY-SA](https://creativecommons.org/licenses/by-sa/4.0/) license.*



## Corresponding Author:

Wan Noraishah Wan Abdul Munim

School of Electrical Engineering, College of Engineering, Universiti Teknologi MARA (UiTM)

Shah Alam, Selangor, Malaysia

Email: aishahmunim@uitm.edu.my

## 1. INTRODUCTION

Over the past 30 years, research into multi-phase motor drives has steadily advanced. A recent and prominent development involves configuring these drives as interconnected three-phase units, all operating within a single magnetic circuit [1]. Multi-phase drives offer several advantages over conventional three-phase drives, including the capacity to manage higher power by distributing it across multiple phases, reduced torque ripple, and improved reliability. Notably, in contrast to a three-phase system, the loss of a single stator phase does not hinder the machine's startup or operation. Additionally, multi-phase systems contribute benefits such as higher torque per ampere for machines of the same size, lower stator copper losses, and diminished rotor harmonic currents [2]. If the sets of windings consist of three-phase configurations, then the analyzed machine is categorized as a multiple three-phase winding machines. Presently, this configuration is widely favored in various applications due to its resemblance to well-established three-phase machine topologies [3]. Consequently, electrical vehicles (EVs) [4], aerospace systems [5], renewable energy generation [6], and

industrial high-power drives [7] are optimal for the implementation of these multi-phase drives. The advancement of the multi-phase domain is propelled by these particular industrial applications. The multi-phase concept, in turn, facilitates a decrease in the count of semiconductor switches and other components, potentially enhancing overall reliability. Nevertheless, in these applications, ensuring continuous operation is crucial, even in the face of potential failures in the inverter, motor/generator, and control system [8]. The higher number of phases in multi-phase motors provides additional degrees of freedom, enabling more sophisticated control strategies and potentially enhancing performance in various aspects compared to traditional three-phase motors.

In various articles, problems connected with the faulted operation of the system with mechanical faults of the drive are presented and described. The main problem in the system is rotor and stator fault identification and compensation [9]. While, in multi-phase induction machines and even three-phase induction machine drive systems, some recent research efforts have been focused on the fault-tolerant machine design [10]-[13], fault detection [14], [15], and fault-tolerant control system [16], [17]. In recent years, fault-tolerant control systems have emerged as a highly active area of research for numerous investigators [18]-[20]. The primary objective of fault-tolerant control is to guarantee the continuous functionality of a system, even in the event of a fault. Three-phase drives remain popular in electrical drive applications due to their practicality [21]. However, these systems face certain limitations, such as high torque ripple during six-step switching and restricted current handling capacity of power switches [22]. In comparison, multi-phase drives offer notable advantages, including reduced current per phase without raising voltage, minimized DC harmonics, and enhanced overall reliability. Despite these benefits, operating induction machines is more complex than DC motors, lacking precision control due to coupled flux and torque components in their input current. Nevertheless, the intricate nonlinear dynamic performance of induction machines can be significantly enhanced using the indirect field-oriented control (IRFOC) theory, enabling separate control of torque and flux.

Another crucial consideration for multi-phase machines is the impact of DC-bus voltage limitations on the maximum achievable output torque under optimal current control with some phases open [23]. While previous studies have analyzed the DC-bus utilization of a multi-phase voltage source inverter (VSI) under balanced conditions [24], fault scenarios often involve optimal current control. Additionally, assumptions of complete decoupling between different subspaces may not hold, especially considering the influence of neutral configuration on low-order current/voltage harmonics [25]. To address these complexities, simple closed-form expressions are proposed to estimate the maximum line voltage determining the maximum achievable torque under various post-fault control strategies and neutral configurations. The same expressions are utilized to estimate the minimum required DC-link voltage magnitude based on the adopted post-fault scenario for the multi-phase induction machine.

Beyond current limits, voltage constraints are critical in defining machine performance, particularly concerning the maximum achievable speed and power. Despite this, discussions on voltage constraints in multi-phase machines during open-phase fault (OPF) remain limited. Unlike current limits, voltage constraints in induction machines are influenced by specific machine parameters, necessitating an accurate method for parameter estimation to determine post-fault voltage limits effectively. This study aims to analyze the performance of multi-phase induction machine drive systems, with a focus on establishing the best approach for incorporating fault-tolerant features in multi-phase drives. The unique contribution of this research is in identifying post-fault current and voltage constraints for symmetrical six-phase induction machines (S6-IM and D3-IM) with configurations of single and dual isolated neutrals under 1OPF. Additionally, the impact of slip frequency ( $\omega_{slip}$ ) and synchronous frequency ( $\omega_s$ ) is assessed. Results reveal that, for the S6-IM considered here, the current constraint is generally reached before the voltage constraint in most fault cases, indicating that current limits primarily restrict post-fault operation. Conversely, in the D3-IM, voltage constraints are usually encountered first. Understanding these limits aids engineers in developing robust control systems, preventing machine failures, and prolonging machine life while ensuring safe and efficient operation.

## 2. SIX-PHASE INDUCTION MACHINES DRIVE SYSTEM

Over time, numerous fault-tolerant control strategies have emerged for multi-phase machines [26], including those with six phases [27]-[30]. Additionally, various controllers have been developed specifically for handling open-phase faults (OPF), such as scalar V/F [31], [32] direct torque control (DTC) [33], [34] and model-based predictive control (MPC) [35]. Despite the diversity of approaches, the majority of these methods rely on field-oriented control (FOC) [36], [37] where machine phase variables undergo transformation into either a stationary or rotating reference frame. This transformation, facilitated by a suitable matrix, is then regulated using controllers like proportional-integral (PI), proportional-resonant (PR), or predictive controllers. There are two main approaches to FOC: direct rotor FOC and indirect rotor FOC. These two approaches differ in how they determine the rotor angle. So, this paper will use indirect rotor FOC (IRFOC) as the controlling mechanism for the six-phase machines.

### 2.1. Six-phase machines windings

The six-phase drive consists of a six-phase induction motor equipped with two independent three-phase winding sets ( $a_1b_1c_1$  and  $a_2b_2c_2$ ), each powered separately by two insulated-gate bipolar transistor (IGBT)-based two-level voltage source converters (VSC1 and VSC2). Windings 1 and 2 are connected in a star configuration, as shown in Figure 1(a), with the neutrals,  $n_1$  and  $n_2$ , either kept isolated for a two-neutral (2N) setup or joined in a single-neutral (1N) configuration. Typically, the three-phase windings 1 and 2 are viewed as spatially displaced by an angle, denoted as  $\gamma$ , illustrated in Figure 1(b) for the S6-IM and Figure 1(c) for the D3-IM. The main types of six-phase machines are defined by  $\gamma$  values:  $\gamma = 60^\circ$  for S6-IM and  $\gamma = 0^\circ$  for D3-IM.

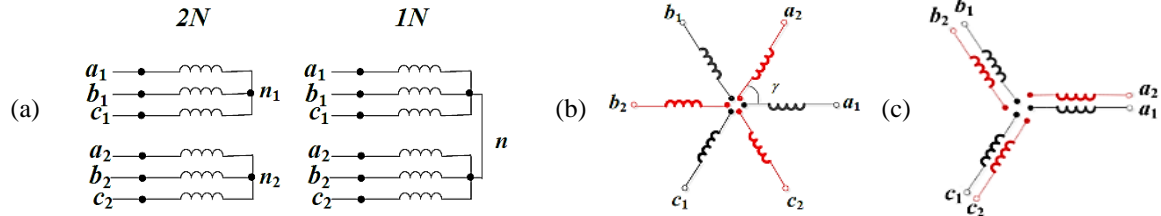


Figure 1. Six-phase machine windings: (a) single and two neutrals connection, (b) S6-IM, and (c) D3-IM that spatially displaced by an arbitrary angle,  $\gamma$  between three-phase windings

### 2.2. The limits of current

For a healthy drive, the current limit is established based on the rated phase current, which is observed when the machine operates at its rated synchronous frequency ( $\omega_s$ ) and rated slip frequency ( $\omega_{slip}$ ). Under normal conditions, the machine's operation is controlled by managing the  $\alpha$ - $\beta$  current components while ensuring that the  $x$ - $y$  and zero-sequence components remain at zero. To evaluate machine performance following a fault, the derating factor, denoted as  $a$ , is applied. This factor represents the per-unit value of the modulus of the post-fault  $\alpha$ - $\beta$  current phasor, with a constraint that the maximum phase current post-fault does not surpass the rated phase current [34], formulated as (1).

$$a = \frac{|I_{\alpha\beta}|_{post-fault}}{|I_{\alpha\beta}|_{Rated}} \quad (1)$$

The derating factor, denoted as  $a$ , is used to evaluate the post-fault torque capacity of a machine with a specific fault while ensuring it remains within the standard current limit. A larger derating factor indicates that a higher maximum torque can be attained while still respecting the current limit restriction.

### 2.3. The limits of voltage

Recent studies, such as article [38], have examined the fault-tolerant control performance of three-phase induction motor drives with respect to current and voltage constraints. For fault-tolerant multi-phase machines, research has explored DC-link voltage limitations under certain open-phase conditions to achieve optimal current in the remaining operational phases [24]. Furthermore, the maximum utilization of the DC-bus voltage within the linear modulation range for normal operation is defined when the peak line voltage matches the DC-bus voltage. In a star-connected six-phase machine, the voltage limit can vary depending on whether the neutrals are connected in a 1N or 2N configuration.

## 3. MATHEMATICAL MODELLING OF SIX-PHASE INDUCTION MACHINES

### 3.1. Vector space decomposition model

Using the vector space decomposition (VSD) method and the generalized Clarke transformation matrix, the phase currents can be broken down into  $\alpha$ ,  $\beta$ ,  $x$ ,  $y$ ,  $0_+$ , and  $0_-$  components, as represented by (2).

$$[\alpha \ \beta \ x \ y \ 0_+ \ 0_-]^T = [T6] \cdot [a_1 \ b_1 \ c_1 \ a_2 \ b_2 \ c_2]^T \quad (2)$$

In this paper, the commonly utilized six-phase decoupling transformation matrices for S6-IM and D3-IM machines are employed, as provided in (3) [39], where  $\gamma$  = arbitrary angle and  $\theta = 2\pi/3$ .

$$[T6] = \frac{1}{\sqrt{3}} \cdot \begin{bmatrix} 1 & \cos(\theta) & \cos(2\theta) & \cos(\gamma) & \cos(\theta + \gamma) & \cos(2\theta + \gamma) \\ 0 & \sin(\theta) & \sin(2\theta) & \sin(\gamma) & \sin(\theta + \gamma) & \sin(2\theta + \gamma) \\ 1 & \cos(2\theta) & \cos(\theta) & -\cos(\gamma) & -\cos(\theta + \gamma) & -\cos(2\theta + \gamma) \\ 0 & \sin(2\theta) & \sin(\theta) & \sin(\gamma) & \sin(\theta + \gamma) & \sin(2\theta + \gamma) \\ 1/\sqrt{2} & 1/\sqrt{2} & 1/\sqrt{2} & 1/\sqrt{2} & 1/\sqrt{2} & 1/\sqrt{2} \\ 1/\sqrt{2} & 1/\sqrt{2} & 1/\sqrt{2} & -1/\sqrt{2} & -1/\sqrt{2} & -1/\sqrt{2} \end{bmatrix} \quad (3)$$

Applying the established VSD framework, the voltage equations in the  $\alpha$ - $\beta$  subspace can be expressed as functions of machine parameters, along with stator and rotor flux, and stator, and rotor currents. In (4)-(7), the parameters  $R_r$ ,  $R_s$ ,  $L_r$ ,  $L_s$ , and  $L_m$  represent the rotor resistance, stator resistance, rotor inductance, stator inductance, and magnetizing inductance respectively, with the symbol  $\hat{\cdot}$  indicating theoretical values of voltages and flux. Within the IRFOC strategy, rotor quantities cannot be directly measured and therefore must be estimated using the machine parameters, necessitating their removal from the voltage equations. By leveraging (8) and (9), the  $\alpha$ - $\beta$  voltages for the induction machine are defined in terms of machine parameters, stator currents, and operating conditions.

$$\hat{v}_{\alpha s} = R_s \cdot i_{\alpha s} + \frac{d}{dt} \hat{\psi}_{\alpha s}; \hat{\psi}_{\alpha s} = L_s \cdot i_{\alpha s} + L_m \cdot i_{ar} \quad (4)$$

$$\hat{v}_{\beta s} = R_s \cdot i_{\beta s} + \frac{d}{dt} \hat{\psi}_{\beta s}; \hat{\psi}_{\beta s} = L_s \cdot i_{\beta s} + L_m \cdot i_{\beta r} \quad (5)$$

$$0 = R_r \cdot i_{ar} + \frac{d}{dt} \hat{\psi}_{ar} + \omega_r \hat{\psi}_{\beta r}; \hat{\psi}_{ar} = L_s \cdot i_{ar} + L_m \cdot i_{\alpha s} \quad (6)$$

$$0 = R_r \cdot i_{\beta r} + \frac{d}{dt} \hat{\psi}_{\beta r} - \omega_r \hat{\psi}_{ar}; \hat{\psi}_{\beta r} = L_s \cdot i_{\beta r} + L_m \cdot i_{\beta s} \quad (7)$$

$$\hat{v}_{\alpha s} = \left( R_s + \frac{L_m^2 \cdot \omega_s \cdot \omega_{slip}}{R_r \left( 1 + \frac{L_r^2 \cdot \omega_{slip}^2}{R_r^2} \right)} \right) \cdot i_{\alpha s} - \left( \sigma \cdot L_s \cdot \omega_s + \frac{L_m^2 \cdot \omega_s}{L_r \left( 1 + \frac{L_r^2 \cdot \omega_{slip}^2}{R_r^2} \right)} \right) \cdot i_{\beta s}; \sigma = 1 - L_m^2 / L_s L_r \quad (8)$$

$$\hat{v}_{\beta s} = \left( \sigma \cdot L_s \cdot \omega_s + \frac{L_m^2 \cdot \omega_s}{L_r \left( 1 + \frac{L_r^2 \cdot \omega_{slip}^2}{R_r^2} \right)} \right) \cdot i_{\alpha s} + \left( R_s + \frac{L_m^2 \cdot \omega_s \cdot \omega_{slip}}{R_r \left( 1 + \frac{L_r^2 \cdot \omega_{slip}^2}{R_r^2} \right)} \right) \cdot i_{\beta s}; \omega_{slip} = \omega_s - \omega_r \quad (9)$$

The voltages in the  $x$ - $y$  and  $0$ - subspaces can be calculated using currents and machine parameters. In contrast to the  $\alpha$ - $\beta$  subspace, the equations for the  $x$ - $y$  and  $0$ - voltages are much simpler, as they do not involve any rotor components, as shown in (10)-(12):

$$\hat{v}_{xs} = R_s \cdot i_{xs} + L_{lsxy} \cdot \frac{d}{dt} i_{xs} \quad (10)$$

$$\hat{v}_{ys} = R_s \cdot i_{ys} + L_{lsxy} \cdot \frac{d}{dt} i_{ys} \quad (11)$$

$$\hat{v}_{0-s} = R_s \cdot i_{0-s} + L_{ls0-} \cdot \frac{d}{dt} i_{0-s} \quad (12)$$

The machine parameters  $L_{ls0-}$  and  $L_{lsxy}$  are the stator leakage inductance for  $0$ - and  $x$ - $y$ .

### 3.2. Process of parameter estimation

Figure 2 presents the comprehensive method for estimating machine parameters. The parameter estimation approach begins with the  $x$ - $y$  subspaces, proceeds with the  $0$ - subspace estimation for a six-phase induction machine in a 1N configuration, and concludes with the  $\alpha$ - $\beta$  subspaces. According to (10)-(12), the parameters  $L_{ls0-}$ ,  $L_{lsxy}$ , and  $\omega_s$  represent the stator leakage inductance for the  $0$ - subspace,  $x$ - $y$  subspace, and the synchronous frequency, respectively. During post-fault operation,  $x$ - $y$  and  $0$ - currents can be expressed in terms of  $\alpha$ - $\beta$  currents, using coefficients K1-K8 as outlined in (13)-(15):

$$\hat{v}_{xs} = A \cdot i_{\alpha s} + B \cdot i_{\beta s} \quad (13)$$

$$\hat{v}_{ys} = C \cdot i_{\alpha s} + D \cdot i_{\beta s} \quad (14)$$

$$\hat{v}_{0-s} = E \cdot i_{\alpha s} + F \cdot i_{\beta s} \quad (15)$$

Based on  $\alpha$ - $\beta$  currents for the induction motor, it will be simplified the  $x$ - $y$  and  $0$ - voltage as in (16)-(21).

$$A = R_s \cdot K_1 + \omega_s \cdot L_{ls\ xy} \cdot K_2 \quad (16)$$

$$B = R_s \cdot K_2 - \omega_s \cdot L_{ls\ xy} \cdot K_1 \quad (17)$$

$$C = R_s \cdot K_3 + \omega_s \cdot L_{ls\ xy} \cdot K_4 \quad (18)$$

$$D = R_s \cdot K_4 - \omega_s \cdot L_{ls\ xy} \cdot K_3 \quad (19)$$

$$E = R_s \cdot K_7 + \omega_s \cdot L_{ls\ 0} \cdot K_8 \quad (20)$$

$$F = R_s \cdot K_8 - \omega_s \cdot L_{ls\ 0} \cdot K_7 \quad (21)$$

The machine is initially operated in pseudo-optimal power factor mode at 1400 rpm, using rated control voltage,  $\omega_{slip}$ , and  $\omega_s$ . The load is increased gradually until the phase current reaches its rated threshold while maintaining the flux current at 1.3 A. Measurements for control currents, voltages, and synchronous frequency are gathered over one fundamental cycle, and then exported to excel for parameter optimization. In Excel, Solver is employed to fine-tune machine parameters ( $R_s$ ,  $L_{ls0}$ , and  $L_{lsxy}$ ) by reducing discrepancies between observed and theoretical voltages in the  $0$ - and  $x$ - $y$  subspaces. Subsequently, parameters in the  $\alpha$ - $\beta$  plane ( $L_m$ ,  $R_r$ ,  $L_{lr\alpha\beta}$ , and  $L_{ls\alpha\beta}$ ) are determined, assuming that the stator resistance ( $R_s$ ) is consistent with that derived from the  $x$ - $y$  subspace. Initial estimates are used to compute theoretical  $\alpha$ - $\beta$  voltages, and further optimization is conducted using excel solver. Unlike in the  $x$ - $y$  subspace,  $\alpha$ - $\beta$  parameters are sensitive to the machine's operating conditions, particularly synchronous and slip frequencies. When  $\omega_s$  and  $\omega_{slip}$  are high, the magnetizing branch becomes dominant, while at lower  $\omega_s$  and  $\omega_{slip}$  values, the rotor branch exerts a more significant influence. To address these variations, optimization is performed under two distinct conditions: High  $\omega_s$  and  $\omega_{slip}$  (1400 rpm with rated  $i_q = 3.3$  A) and Low  $\omega_s$  and  $\omega_{slip}$  (350 rpm at no load,  $i_q = 0.5$  A), akin to locked-rotor and no-load tests. Finally, machine parameters from all subspaces are utilized to calculate theoretical voltages.

### 3.3. Fault-tolerant strategy based on maximum torque (MT)

Maintaining the nominal current limit is essential for the inverter, which is generally set to operate with a capped current value to protect the drive, even in fault conditions. When applying the maximum torque (MT) strategy during post-fault, the objective is to minimize the peak phase current in the remaining functional phases. Several methods are available to optimize post-fault currents; here, we adopt the approach outlined in [16], which relies on decoupled variables. The coefficient 'K' is used to define the relationship between non-energy-converting currents and the  $\alpha$ - $\beta$  references. For a six-phase machine, optimization is required only for the  $x$ - $y$  currents and the zero-sequence current,  $0$ - as shown in (22)-(25), with zero-sequence  $0+$  set to zero, leading to K5 and K6 being equal to 0.

$$i_x^* = K_1 \cdot i_a^* + K_2 \cdot i_b^* \quad (22)$$

$$i_y^* = K_3 \cdot i_a^* + K_4 \cdot i_b^* \quad (23)$$

$$i_{0+}^* = K_5 \cdot i_a^* + K_6 \cdot i_b^* \quad (24)$$

$$i_{0-}^* = K_7 \cdot i_a^* + K_8 \cdot i_b^* \quad (25)$$

A non-linear optimization technique, specifically the generalized reduced gradient (GRG) method available in the "Solver" tool in MS Office Excel, is applied to optimize post-fault currents. For maximum torque (MT) modes, the optimization objectives are drawn from (26) and serve as the cost function,  $J_{MT}$ , with the goal of maximizing torque. This involves maximizing the  $\alpha$ - $\beta$  phasor amplitude while adhering to the constraints listed in (27).

$$J_{MT} = \max |I_{\alpha\beta}| \quad (26)$$

$$\begin{aligned} I_{fault} &= 0 \in \{Faulted\ phases\} \\ i_{0+} &= 0; \min \text{ the max phase current } \in \{healthy\ phases\} \end{aligned} \quad (27)$$

Tables 1 and 2 illustrate the connection between  $\alpha$ - $\beta$ ,  $x$ - $y$ ,  $0$ -, and  $0$ + currents across all fault scenarios and neutral configurations for the S6-IM and D3-IM, respectively. The implementation of coefficients K1-K8 in the equation signifies the influence of zero sequence current and  $x$ - $y$  components on post-fault execution.

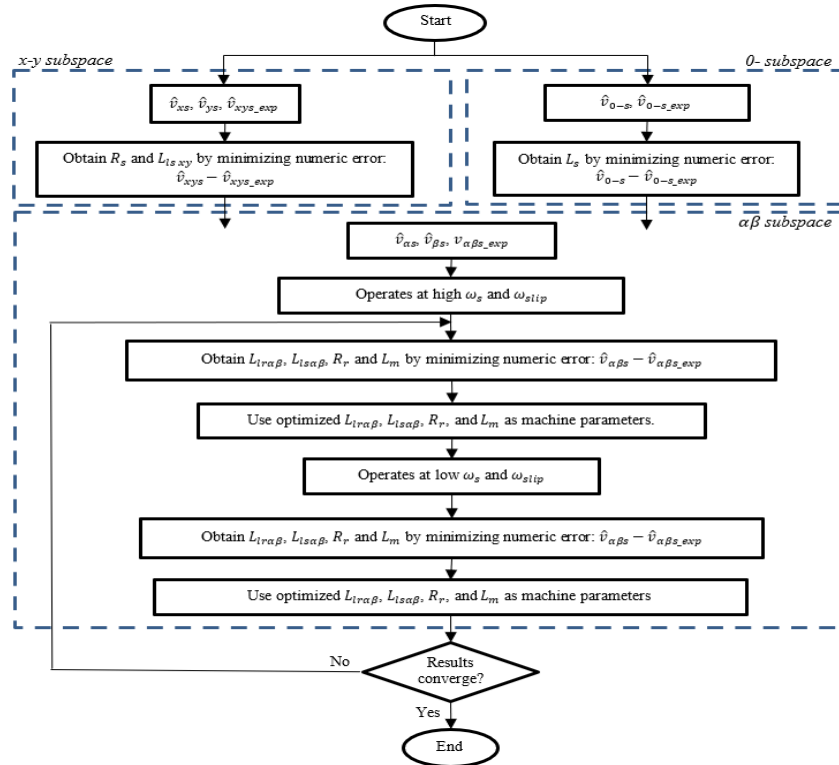


Figure 2. Parameter estimation flowchart

Table 1. Post-fault strategy based on  $x$ - $y$ ,  $0$ -, and  $0$ + current components reconfiguration over 1OPF scenario during 2N and 1N for S6-IM

Case		Coefficients, K								$\alpha$
	Healthy	K1	K2	K3	K4	K5	K6	K7	K8	
Faulty phase (1N)	1OPF	-0.648	0	0	-0.368	0	0	-0.497	0	0.771
Faulty phase (2N)	1OPF	-1	0	0	-0.333	0	0	0	0	0.500

Table 2. Post-fault strategy based on  $x$ - $y$ ,  $0$ -, and  $0$ + current components reconfiguration over 1OPF scenario during 2N and 1N for D3-IM

Case		Coefficients, K								$\alpha$
	Healthy	K1	K2	K3	K4	K5	K6	K7	K8	
Faulty phase (1N)	1OPF	-0.667	0.577	1.732	0	0	0	-0.471	-0.817	0.500
Faulty phase (2N)	1OPF	-1	0	0	-0.333	0	0	0	0	0.500

#### 4. POST-FAULT PERFORMANCE FOR SIX-PHASE IM UNDER DIFFERENT OPERATING POINT

It is important to keep in mind that based on operating points the maximum line-to-line voltage can vary, particularly  $\omega_s$  and  $\omega_{slip}$ . Understanding how line-to-line voltage varies with these parameters is important. The  $\omega_s$  is defined as shown in (28).

$$\omega_s = 2\pi f \quad (28)$$

When operating up to the base speed, the frequency ( $f$ ) matches the rated frequency when the maximum value of  $\omega_s$  is reached. For a 50 Hz induction machine, the peak  $\omega_s$  equals 314 rad/s. Conversely,  $\omega_{slip}$  depends on factors such as the rotor time constant,  $i_{qs}$  and  $i_{ds}$  as detailed in (29).

$$\omega_{slip} = \frac{1}{\tau_r} \cdot \frac{i_{qs}}{i_{ds}}; \tau_r = \frac{L_r}{R_r} \quad (29)$$

The maximum slip frequency can be determined as a function of  $i_{qs}$ ,  $i_{ds}$  up to the rated condition, and the derating factor,  $a$  as specified in (30) and (31).

$$\begin{aligned} |i_{dqs}'| &\leq a|i_{dqs}|_{rated} \\ \sqrt{i_{ds}'^2 + i_{qs}'^2} &\leq a|i_{dq}|_{rated} \quad ; \quad k = a|i_{dqs}|_{rated} \end{aligned} \quad (30)$$

$$\begin{aligned} \sqrt{i_{dsrated}^2 + (\tau_r \cdot i_{dsrated} \cdot \omega_{slip})^2} &\leq k \quad \therefore \omega_{slip} \leq \sqrt{\frac{k^2 - i_{dsrated}^2}{\tau_r^2 \cdot i_{dsrated}^2}} \\ \omega_{slipmax} &= \sqrt{\frac{a^2|i_{dqs}|_{rated}^2 - i_{dsrated}^2}{\tau_r^2 \cdot i_{dsrated}^2}} = \sqrt{\frac{a^2(i_{dsrated}^2 + i_{qsrated}^2) - i_{dsrated}^2}{\tau_r^2 \cdot i_{dsrated}^2}} \\ &= \sqrt{(a\omega_{sliprated})^2 - \left(\frac{1-a^2}{\tau_r^2}\right)} \end{aligned} \quad (31)$$

Yet, the maximum slip frequency,  $\omega_{slipmax}$ , is only valid under the condition specified in (32).

$$\alpha_{min} \cdot I_{srated} > I_{drated} \quad (32)$$

## 5. RESULT AND DISCUSSIONS

The performance of an electrical machine is influenced not just by current limits but by voltage constraints also. These voltage limits are connected to the inverter's ability to provide the required voltages to the machine, which are primarily determined by the design of the inverter, the winding configuration of the machine, and the DC-link voltage. Once the post-fault currents are determined, the voltage necessary to produce these currents is affected by both the derating factor and the machine's parameters, as shown earlier in Tables 1 and 2. Table 3, on the other hand, summarizes the machine parameters used for the S6-IM and D3-IM models. With the given voltage equations and machine parameters, the voltages for the machine's decoupled subspaces can be computed based on the post-fault currents and operating conditions. The post-fault phase voltages can be derived by applying the inverse Clarke transformation to the components  $v_{\alpha-\beta, x-y, 0+0-}$ . The post-fault line-to-line voltages are calculated by finding the differences between these phase voltages, enabling the determination of the maximum line-to-line voltage under different fault operating scenarios. Therefore, the results will be presented in two sections, based on the voltage limit relative to  $\omega_s$  and  $\omega_{slip}$  approach.

Table 3. Machine parameters for S6-IM and D3-IM

Machine parameters	Converter parameters
$R_s = 12.532 \, \Omega$	$\omega_{slip, rated} = 29.04 \, rad/s$
$R_r = 5.776 \, \Omega$	$V_{rated} = 280 \, V$
$L_{lr} = 78 \, mH$	$f = 50 \, Hz$
$L_m = 420 \, mH$	
$L_{ls \, \alpha\beta} = 6 \, mH$	
$L_{ls \, xy} = 3.634 \, mH$	
$L_0 = 6 \, mH$	

### 5.1. Voltage limits in relation to synchronous frequency, $\omega_s$

Under healthy operating conditions, both machine types operate at 1 per unit (p.u.), indicating that none of the phases are experiencing faults. The line-to-line voltages are normalized against the maximum healthy line-to-line voltage for each six-phase machine type. As a result, the voltage limits differ according to the neutral configuration: S6-IM-1N has a limit of 1 p.u., while S6-IM-2N is limited to 0.866 p.u.; both D3-IM-1N and D3-IM-2N have a voltage limit of 1 p.u. It remains unclear whether the voltage limit will be reached prior to the current limit, as the latter could become a limiting factor during post-fault operations. To fully understand the post-fault capabilities of the S6-IM and D3-IM, it is crucial to consider both the current and voltage limits. Consequently, this study explores the post-fault voltage limits for each induction machine type. Figures 3(a)-3(c) illustrates the voltage limits in terms of line-to-line voltages at different values of  $\omega_s$  for the S6-IM machine, while Figures 4(a)-4(c) does the same for the D3-IM machine, both assuming rated current

and  $\omega_{slip}$ . The vertical dashed line in the graphs marks the rated speed, and the horizontal dashed line indicates the voltage limit. All results are based on the post-fault strategy described in Tables 1 and 2.

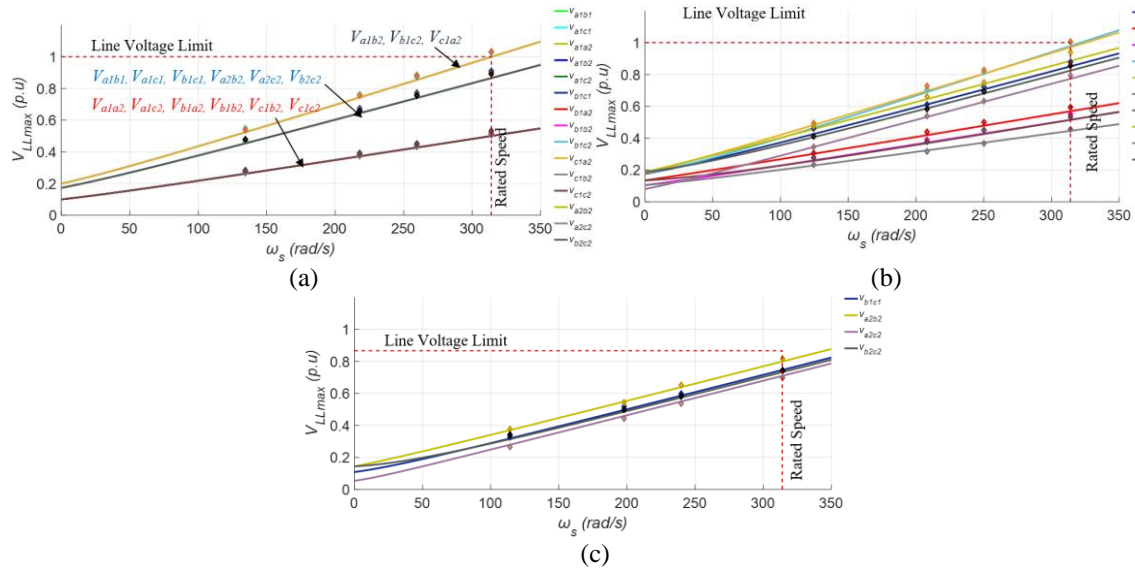


Figure 3. Voltage limit under different  $\omega_s$  at rated  $\omega_{slip}$  and rated current for S6-IM:  
(a) healthy condition, 1OPF under (b) 1N, and (c) 2N configurations

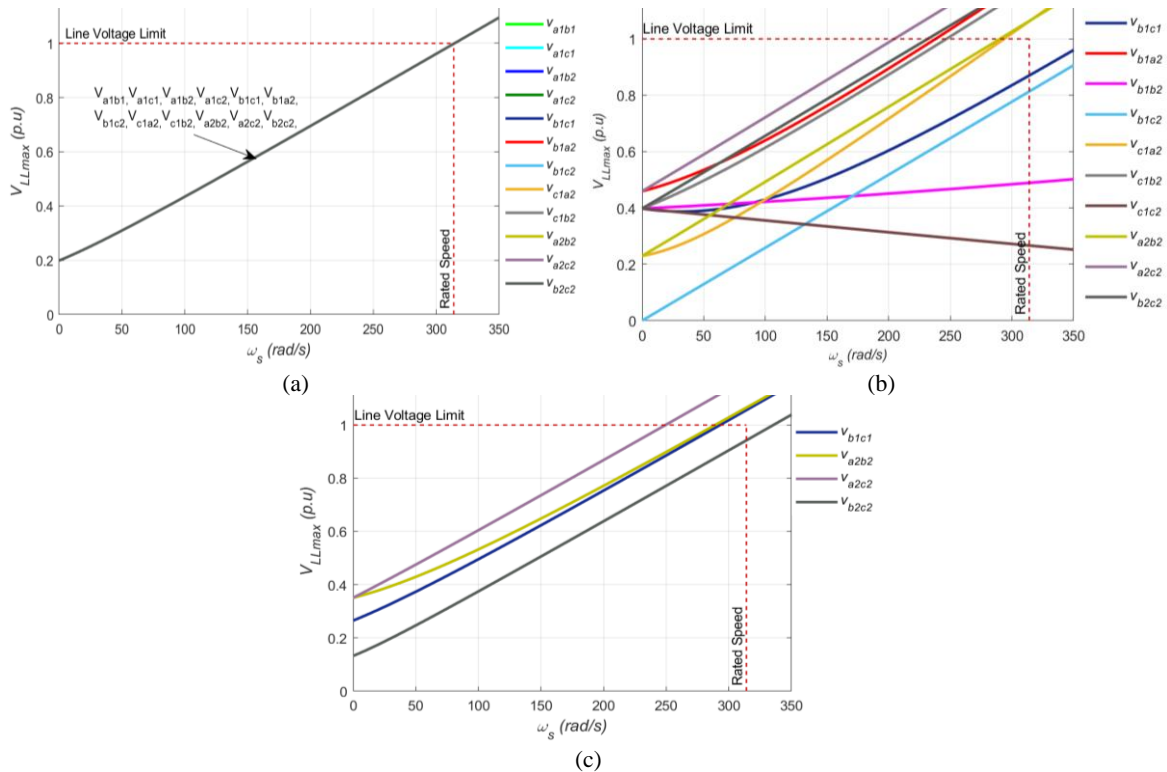


Figure 4. Voltage limit under different  $\omega_s$  at rated  $\omega_{slip}$  and rated current for D3-IM:  
(a) healthy condition, 1OPF under (b) 1N, and (c) 2N configurations

Figure 3(a) illustrates the results for healthy operation under different  $\omega_s$  at rated  $\omega_{slip}$  and rated current of the S6-IM, while Figures 3(b) and 3(c) illustrate the line-to-line voltages for 1OPF with one neutral (1N) and two neutrals (2N), respectively. As shown in Figure 3, it is clear that in 1OPF scenarios, whether under 1N or 2N configurations, the current limit is reached before the voltage limit. Special attention should be given to



the 1OPF with 1N, where the maximum line-to-line voltages almost hit the voltage limit, potentially due to the impact of the  $0$ -subspace.

Figure 4(a) displays the results for a healthy-operated D3-IM, while Figures 4(b) and 4(c) illustrate the line-to-line voltages under 1OPF with 1N and 2N configurations, respectively. The results shown in Figures 4 demonstrate that the voltage limit of D3-IM is reached before the current limit. This indicates that the D3-IM is primarily determined by voltage limitations at different  $\omega_s$  when operating at rated  $\omega_{slip}$  and rated current.

In summary, the S6-IM generally operates within the current limit during most fault scenarios. On the other hand, the D3-IM is entirely controlled by the limitation of voltage across all fault scenarios. One can agree that D3-IM is less aggressive to the machine windings for not working at the current limits; despite this, D3-IM seems to be not able to work at higher speeds. The S6-IM, however, can maintain higher speeds under OPF conditions, making it advantageous in various situations. Comparatively, the S6-IM is considered to have the best fault-tolerant capability based on its voltage limit across different  $\omega_s$  at rated  $\omega_{slip}$  and current. This indicates that the post-fault behavior of the S6-IM is largely governed by the current limit.

## 5.2. Voltage limits in relation to slip frequency, $\omega_{slip}$

From the  $\alpha$ - $\beta$  voltage equations discussed in section 3, it is evident that voltage depends on current, operating conditions, and machine parameters which are primarily influenced by  $\omega_{slip}$  and  $\omega_s$  at rated current. To comprehensively analyze the post-fault performance of each induction machine, it is essential to evaluate the voltage limits across various operating conditions. Tables 4 and 5 provide the maximum slip frequencies for the S6-IM and D3-IM, respectively, considering 2N and 1N configurations under 1OPF scenario.

Table 4. Maximum slip frequency,  $\omega_{slip}$  of S6-IM based on neutral connections for 1OPF scenario

Case	Max $\omega_{slip}$ (rad/s)
Healthy	29.4
Faulty phase (1N) 1OPF	21.43
Faulty phase (2N) 1OPF	10.73

Table 5. Maximum slip frequency,  $\omega_{slip}$  of D3-IM based on neutral connections for 1OPF scenario

Case	Max $\omega_{slip}$ (rad/s)
Healthy	29.04
Faulty phase (1N) 1OPF	14.52
Faulty phase (2N) 1OPF	14.52

In post-fault control, the flux current,  $i_{ds}$  is maintained at its rated value of 1.3 A for both S6-IM and D3-IM machines. The synchronous frequency,  $\omega_s$  is set to 314 rad/s as defined in (28), with  $i_{qs}$  reflecting the torque as described in (29). The slip frequency limit,  $\omega_{slip}$  represents the current constraint for the post-fault machine, ensuring the maximum phase current does not exceed the rated phase current. Consequently, the maximum slip frequency,  $\omega_{slipmax}$  calculated using (31), determines the current limit for 1OPF conditions. On the other hand, the voltage limit is influenced by the neutral configurations. Notably, in scenarios analyzing voltage against  $\omega_{slip}$ , medium line-to-line voltages often surpass large line-to-line voltages. This phenomenon is mainly attributed to the impact of the  $x$ - $y$  and  $0$ -components, leading to uneven  $\omega_{slip}$  effects on line-to-line voltages. Figures 5 and 6 illustrate these voltage constraints as line-to-line voltages across different  $\omega_{slip}$  scenarios at rated  $\omega_s$  and current for S6-IM and D3-IM, respectively. In these figures, the vertical dashed line indicates the rated values for various fault conditions, with the derating factor,  $a$  representing the current limit, while the horizontal dashed line denotes the voltage limit.

Figure 5(a) illustrates the outcomes of healthy operation for S6-IM, whereas Figures 5(b) and 5(c) display the line-to-line voltages under 1OPF scenario with 1N and 2N configurations, respectively. Under rated  $\omega_s$ , it is observed that, the current limit of maximum line voltages is reached before the voltage limit. Notably, for 1OPF under 1N for S6-IM, the maximum line-to-line voltages nearly reach the voltage limit due to the influence of the  $0$ -subspace same as results in section 5.1. Figure 6(a) illustrates the results for a healthy-operated D3-IM, while Figures 6(b) and 6(c) depict the line-to-line voltages under 1OPF with 1N and 2N configurations, respectively. Upon analysis of the results for the D3-IM, it is observed that under fault scenarios with 2N, the maximum line-to-line voltages reach the current limit first. Conversely, for fault scenarios where D3-IM is configured with 1N, the maximum line-to-line voltages hit the voltage limit before reaching the current limit. In conclusion, D3-IM with 2N is primarily influenced by the limitation of current, while with 1N, voltage becomes the limiting factor.

In summary, S6-IM predominantly operates within the current limit during most fault scenarios. Conversely, D3-IM is consistently controlled by the demonstrates superior fault-tolerant capability based on its voltage limit under different  $\omega_{slip}$  at rated  $\omega_s$  and current. Overall, voltage limitation helps to control the damage due to overcurrent [39]. By using this control method instead of the current control, synchronization instability can be avoided. This instability is typically caused by the limitations on how long the current can remain at a saturated level. In contrast, voltage control does not impose such constraints in various situations.

So, it can be said that S6-IM is the best fault-tolerant capability based on post-fault performance for both approaches which are by using rated  $\omega_{slip}$  as explained in section 5.1 and rated  $\omega_s$ .

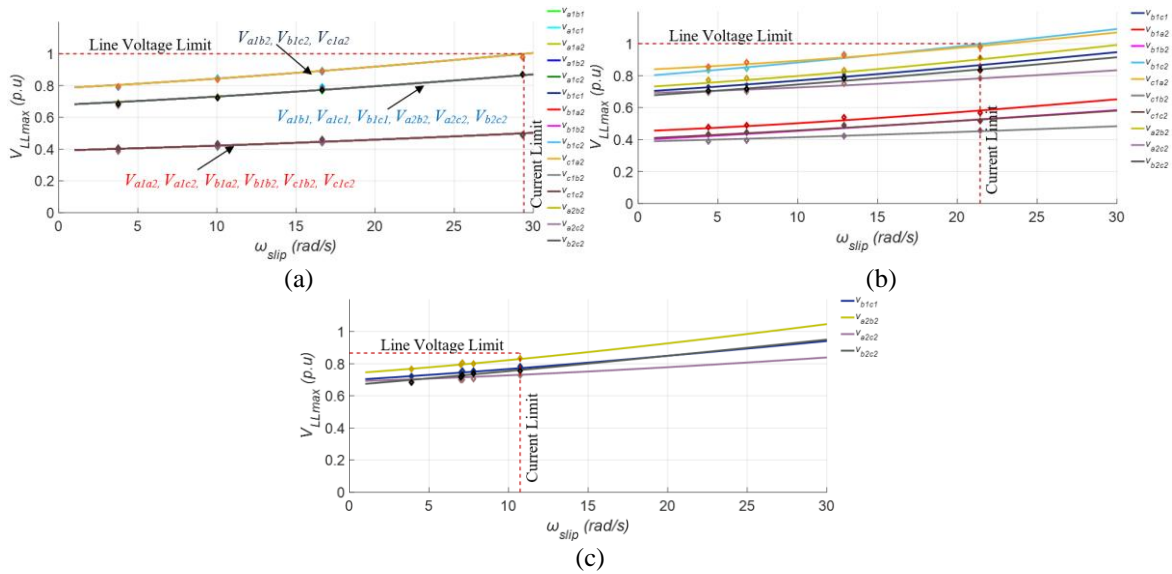


Figure 5. S6-IM voltage limit under different  $\omega_{slip}$  at rated current and  $\omega_s$  during (a) healthy condition, 1OPF under (b) 1N, and (c) 2N configurations

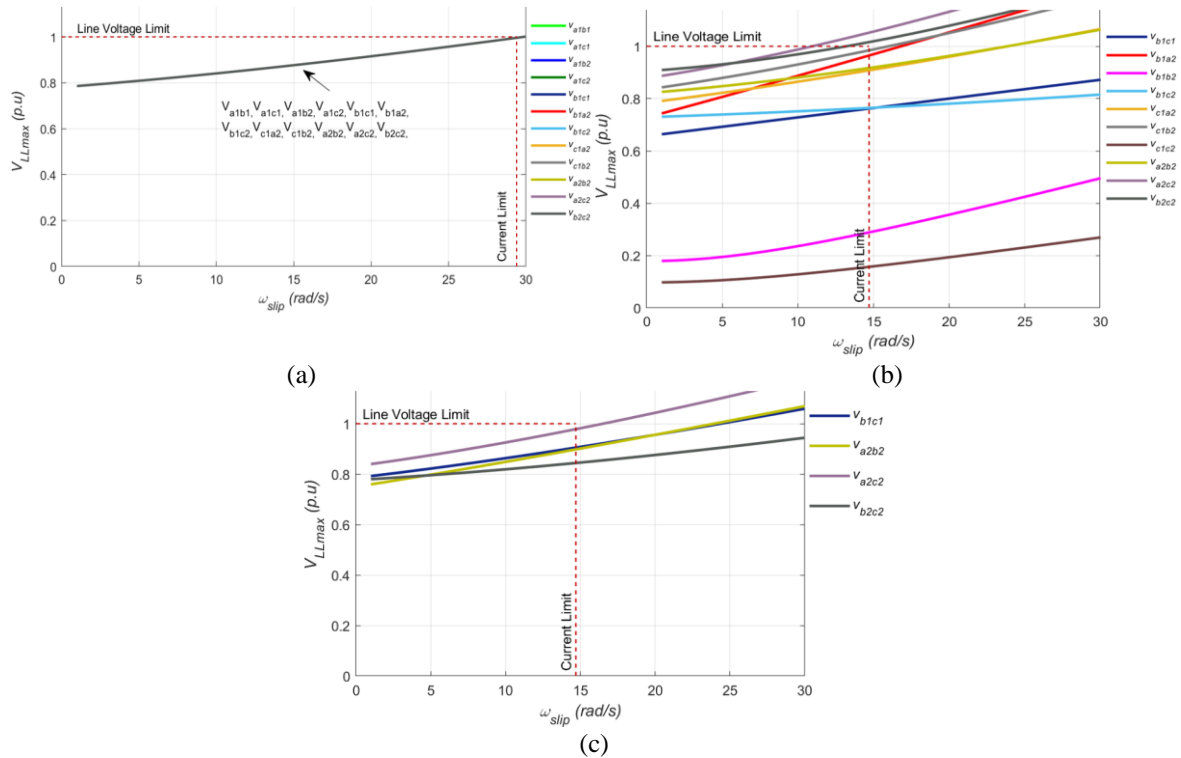


Figure 6. D3-IM voltage limit under different  $\omega_{slip}$  at rated current and  $\omega_s$  during (a) healthy condition, 1OPF under (b) 1N, and (c) 2N configurations

## 6. CONCLUSION

This study investigated how post-fault conditions affect the maximum line-to-line voltage in S6-IM and D3-IM at various synchronous and slip frequency operating points. A simulated line graph was used to show the maximum line voltage versus synchronous frequency under different fault scenarios, helping to

determine whether voltage or current will be the limiting factor first. It was observed that the S6-IM is generally controlled by the current limit when synchronous frequency varies, while the D3-IM is entirely governed by voltage limits under all fault conditions. Similarly, when slip frequency varies, the S6-IM is likely controlled by the current limit, whereas the D3-IM remains controlled by the voltage limit in all scenarios. It should be noted that, the S6-IM is considered to have the best fault-tolerant capability based on its voltage limit across different  $\omega_s$  and  $\omega_{slip}$  approaches. The post-fault performance of the S6-IM is mainly governed by the current limit, whereas for the D3-IM, it is predominantly influenced by the voltage limit across all fault conditions. So, this makes the D3-IM less aggressive on the machine windings due to not reaching the current limits, it is unable to operate at higher speeds. Moreover, one of the most important components of fault tolerance in motor systems is being able to keep voltage within safe bounds when fault conditions occur. To ensure safe and reliable operation under various failure scenarios, a well-designed, fault-tolerant motor system should incorporate efficient control techniques and safety systems.

## ACKNOWLEDGEMENTS

This research is funded by Universiti Teknologi MARA, Malaysia under the Fundamental Research Grant Scheme (FRGS/1/2021/TK0/UITM/02/31). The authors would like to acknowledge College of Engineering, Universiti Teknologi MARA for the excellent facility provided to carry out the research. The authors would also like to express their gratitude to everyone who have either directly or indirectly assisted in the completion of the study.




## REFERENCES

- [1] Z. Liu, Y. Li, and Z. Zheng, "A review of drive techniques for multi-phase machines," *CES Transactions on Electrical Machines and Systems*, vol. 2, no. 2, pp. 243–251, Jun. 2018, doi: 10.30941/CESTEMS.2018.00030.
- [2] R. S. Miranda, C. B. Jacobina, and A. M. N. Lima, "Modeling and analysis of six-phase induction machine under fault condition," in *2009 Brazilian Power Electronics Conference*, IEEE, Sep. 2009, pp. 824–829, doi: 10.1109/COBEP.2009.5347696.
- [3] D. Diallo, M. E. H. Benbouzid, and A. Makouf, "A fault-tolerant control architecture for induction motor drives in automotive applications," *IEEE Transactions on Vehicular Technology*, vol. 53, no. 6, pp. 1847–1855, Nov. 2004, doi: 10.1109/TVT.2004.833610.
- [4] L. Parsa and H. A. Toliyat, "Fault-tolerant interior-permanent-magnet machines for hybrid electric vehicle applications," *IEEE Transactions on Vehicular Technology*, vol. 56, no. 4, pp. 1546–1552, Jul. 2007, doi: 10.1109/TVT.2007.896978.
- [5] G. Sulligoi, A. Tesserolo, V. Benucci, M. Baret, A. Rebora, and A. Taffone, "Modeling, simulation and experimental validation of a generation system for medium-voltage DC integrated power systems," in *2009 IEEE Electric Ship Technologies Symposium*, IEEE, Apr. 2009, pp. 129–134, doi: 10.1109/ESTS.2009.4906505.
- [6] B. Andresen and J. Birk, "A high power density converter system for the Gamesa G10x 4.5 MW wind turbine," in *2007 European Conference on Power Electronics and Applications*, IEEE, 2007, pp. 1–8, doi: 10.1109/EPE.2007.4417312.
- [7] R. R. Bastos, T. S. de Souza, M. M. de Carvalho, L. A. R. Silva, and B. J. C. Filho, "Assessment of a nine-phase induction motor drive for metal industry applications," *IEEE Transactions on Industry Applications*, vol. 56, no. 6, pp. 7217–7226, Nov. 2020, doi: 10.1109/TIA.2020.3023061.
- [8] M. Malinowski, E. Levi, and T. Orlowska-Kowalska, "Introduction to the special section on intelligent fault monitoring and fault-tolerant control in power electronics, drives and renewable energy systems," *Power Electronics and Drives*, vol. 4, no. 1, pp. 163–165, Jun. 2019, doi: 10.2478/pead-2019-0016.
- [9] F. Zidani, D. Diallo, M. E. H. Benbouzid, and E. Berthelot, "Diagnosis of speed sensor failure in induction motor drive," in *2007 IEEE International Electric Machines & Drives Conference*, IEEE, May 2007, pp. 1680–1684, doi: 10.1109/IEMDC.2007.383682.
- [10] G. Zhang, W. Hua, M. Cheng, and J. Liao, "Design and comparison of two six-phase hybrid-excited flux-switching machines for EV/HEV applications," *IEEE Transactions on Industrial Electronics*, vol. 63, no. 1, pp. 481–493, 2016, doi: 10.1109/TIE.2015.2447501.
- [11] A. S. Abdel-Khalik, M. A. Elgenedy, S. Ahmed, and A. M. Massoud, "An improved fault-tolerant five-phase induction machine using a combined star/pentagon single layer stator winding connection," *IEEE Transactions on Industrial Electronics*, vol. 63, no. 1, pp. 618–628, Jan. 2016, doi: 10.1109/TIE.2015.2426672.
- [12] A. Cavagnino, Z. Li, A. Tenconi, and S. Vaschetto, "Integrated generator for more electric engine: design and testing of a scaled-size prototype," *IEEE Transactions on Industry Applications*, vol. 49, no. 5, pp. 2034–2043, Sep. 2013, doi: 10.1109/TIA.2013.2259785.
- [13] W. N. W. A. Munim, M. Tousizadeh, and H. S. Che, "Effects of zero-sequence transformations and min-max injection on fault-tolerant symmetrical six-phase drives with single isolated neutral," *Journal of Power Electronics*, vol. 19, no. 4, pp. 968–979, 2019, doi: 10.6113/JPE.2019.19.4.968.
- [14] W. N. W. A. Munim, H. S. Che, M. Tousizadeh, R. Baharom, and K. S. Muhammad, "Modeling of six-phase induction machine with two isolated neutrals under one open phase fault," in *2022 IEEE Industrial Electronics and Applications Conference (IEACon)*, IEEE, Oct. 2022, pp. 99–104, doi: 10.1109/IEACon55029.2022.9951719.
- [15] A. Pantea *et al.*, "Six-phase induction machine model for electrical fault simulation using the circuit-oriented method," *IEEE Transactions on Industrial Electronics*, vol. 63, no. 1, pp. 494–503, Jan. 2016, doi: 10.1109/TIE.2015.2493727.
- [16] H. S. Che, M. J. Duran, E. Levi, M. Jones, W.-P. Hew, and N. Abd. Rahim, "Postfault operation of an asymmetrical six-phase induction machine with single and two isolated neutral points," *IEEE Transactions on Power Electronics*, vol. 29, no. 10, pp. 5406–5416, Oct. 2014, doi: 10.1109/TPEL.2013.2293195.
- [17] I. Gonzalez-Prieto, M. J. Duran, H. S. Che, E. Levi, M. Bermudez, and F. Barrero, "Fault-tolerant operation of six-phase energy conversion systems with parallel machine-side converters," *IEEE Transactions on Power Electronics*, vol. 31, no. 4, pp. 3068–3079, Apr. 2016, doi: 10.1109/TPEL.2015.2455595.
- [18] W. N. W. A. Munim, M. J. Duran, H. S. Che, M. Bermudez, I. Gonzalez-Prieto, and N. A. Rahim, "A unified analysis of the fault tolerance capability in six-phase induction motor drives," *IEEE Transactions on Power Electronics*, vol. 32, no. 10, pp. 7824–7836, Oct. 2017, doi: 10.1109/TPEL.2016.2632118.





- [19] S. Ni, Z. Zheng, and J. Sun, "An online global fault-tolerant control strategy for asymmetrical multi-phase machines with minimum losses in full torque operation range," in *2022 IEEE Transportation Electrification Conference and Expo, Asia-Pacific (ITEC Asia-Pacific)*, IEEE, Oct. 2022, pp. 1–6, doi: 10.1109/ITECAsia-Pacific56316.2022.9942120.
- [20] A. G. Yepes, M. S. Abdel-Majeed, H. S. Che, A. S. Abdel-Khalik, S. Ahmed, and J. Doval-Gandoy, "DC-signal injection for stator-resistance estimation in symmetrical six-phase induction motors under open-phase fault," *IEEE Transactions on Industrial Electronics*, vol. 70, no. 6, pp. 5444–5453, Jun. 2023, doi: 10.1109/TIE.2022.3192695.
- [21] A. K. Sahoo and R. K. Jena, "Loss model based controller of fuzzy DTC driven induction motor for electric vehicles using optimal stator flux," *e-Prime - Advances in Electrical Engineering, Electronics and Energy*, vol. 6, Dec. 2023, doi: 10.1016/j.prime.2023.100304.
- [22] M. A. Abbas, R. Christen, and T. M. Jahns, "Six-phase voltage source inverter driven induction motor," *IEEE Transactions on Industry Applications*, vol. IA-20, no. 5, pp. 1251–1259, Sep. 1984, doi: 10.1109/TIA.1984.4504591.
- [23] A. S. Abdel-Khalik, M. I. Masoud, S. Ahmed, and A. Massoud, "Calculation of derating factors based on steady-state unbalanced multi-phase induction machine model under open phase(s) and optimal winding currents," *Electric Power Systems Research*, vol. 106, pp. 214–225, Jan. 2014, doi: 10.1016/j.epsr.2013.08.015.
- [24] E. Levi, D. Dujic, M. Jones, and G. Grandi, "Analytical determination of DC-bus utilization limits in multi-phase VSI supplied AC Drives," *IEEE Transactions on Energy Conversion*, vol. 23, no. 2, pp. 433–443, Jun. 2008, doi: 10.1109/TEC.2008.921557.
- [25] A. G. Yepes, J. Doval-Gandoy, F. Baneira, D. Perez-Estevéz, and O. Lopez, "Current harmonic compensation for n -phase machines with asymmetrical winding arrangement and different neutral configurations," *IEEE Transactions on Industry Applications*, vol. 53, no. 6, pp. 5426–5439, Nov. 2017, doi: 10.1109/TIA.2017.2722426.
- [26] W. N. W. A. Munim, H. S. Che, and W. P. Hew, "Fault tolerant capability of symmetrical multi-phase machines under one open-circuit fault," in *IET Conference Publications*, Institution of Engineering and Technology, 2016, pp. 1–6, doi: 10.1049/cp.2016.1333.
- [27] M.-A. Shamsi-Nejad, B. Nahid-Mobarakeh, S. Pierfederici, and F. Meibody-Tabar, "Fault tolerant and minimum loss control of double-star synchronous machines under open phase conditions," *IEEE Transactions on Industrial Electronics*, vol. 55, no. 5, pp. 1956–1965, May 2008, doi: 10.1109/TIE.2008.918485.
- [28] R. Kianinezhad, B. Nahid-Mobarakeh, L. Baghli, F. Betin, and G.-A. Capolino, "Modeling and control of six-phase symmetrical induction machine under fault condition due to open phases," *IEEE Transactions on Industrial Electronics*, vol. 55, no. 5, pp. 1966–1977, May 2008, doi: 10.1109/TIE.2008.918479.
- [29] F. Baudart, B. Dehez, E. Matagne, D. Telteu-Nedelcu, P. Alexandre, and F. Labrique, "Torque control strategy of polyphase permanent-magnet synchronous machines with minimal controller reconfiguration under open-circuit fault of one phase," *IEEE Transactions on Industrial Electronics*, vol. 59, no. 6, pp. 2632–2644, Jun. 2012, doi: 10.1109/TIE.2011.2170393.
- [30] M. J. Duran, I. Gonzalez Prieto, M. Bermudez, F. Barrero, H. Guzman, and M. R. Arahal, "Optimal fault-tolerant control of six-phase induction motor drives with parallel converters," *IEEE Transactions on Industrial Electronics*, vol. 63, no. 1, pp. 629–640, Jan. 2016, doi: 10.1109/TIE.2015.2461516.
- [31] A. S. Abdel-Khalik, A. S. Morsy, S. Ahmed, and A. M. Massoud, "Effect of stator winding connection on performance of five-phase induction machines," *IEEE Transactions on Industrial Electronics*, vol. 61, no. 1, pp. 3–19, Jan. 2014, doi: 10.1109/TIE.2013.2242417.
- [32] A. Sayed-Ahmed and N. A. O. Demerdash, "Fault-tolerant operation of delta-connected scalar- and vector-controlled AC motor drives," *IEEE Transactions on Power Electronics*, vol. 27, no. 6, pp. 3041–3049, Jun. 2012, doi: 10.1109/TPEL.2011.2176556.
- [33] M. Bermudez, I. Gonzalez-Prieto, F. Barrero, H. Guzman, M. J. Duran, and X. Kestelyn, "Open-phase fault-tolerant direct torque control technique for five-phase induction motor drives," *IEEE Transactions on Industrial Electronics*, vol. 64, no. 2, pp. 902–911, Feb. 2017, doi: 10.1109/TIE.2016.2610941.
- [34] Y. Zhou, X. Lin, and M. Cheng, "A fault-tolerant direct torque control for six-phase permanent magnet synchronous motor with arbitrary two opened phases based on modified variables," *IEEE Transactions on Energy Conversion*, vol. 31, no. 2, pp. 549–556, Jun. 2016, doi: 10.1109/TEC.2015.2504376.
- [35] H. Guzman, F. Barrero, and M. J. Duran, "IGBT-gating failure effect on a fault-tolerant predictive current-controlled five-phase induction motor drive," *IEEE Transactions on Industrial Electronics*, vol. 62, no. 1, pp. 15–20, Jan. 2015, doi: 10.1109/TIE.2014.2331019.
- [36] H. S. Che, E. Levi, M. Jones, W.-P. Hew, and N. Abd. Rahim, "Current control methods for an asymmetrical six-phase induction motor drive," *IEEE Transactions on Power Electronics*, vol. 29, no. 1, pp. 407–417, Jan. 2014, doi: 10.1109/TPEL.2013.2248170.
- [37] M. J. Duran, I. Gonzalez-Prieto, N. Rios-Garcia, and F. Barrero, "A simple, fast, and robust open-phase fault detection technique for six-phase induction motor drives," *IEEE Transactions on Power Electronics*, vol. 33, no. 1, pp. 547–557, Jan. 2018, doi: 10.1109/TPEL.2017.2670924.
- [38] M. Tousizadeh, H. S. Che, J. Selvaraj, N. A. Rahim, and B.-T. Ooi, "Performance comparison of fault-tolerant three-phase induction motor drives considering current and voltage limits," *IEEE Transactions on Industrial Electronics*, vol. 66, no. 4, pp. 2639–2648, Apr. 2019, doi: 10.1109/TIE.2018.2850006.
- [39] F. A. Azman, W. N. W. A. Munim, H. S. Che, and A. A. A. Wahab, "Post-fault voltage limit of dual three-phase induction machine against slip frequency with single and two isolated neutrals," in *2022 IEEE International Conference in Power Engineering Application (ICPEA)*, IEEE, Mar. 2022, pp. 1–6, doi: 10.1109/ICPEA53519.2022.9744707.

## BIOGRAPHIES OF AUTHORS







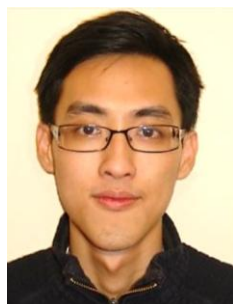
**Nooradzanie Muhammad Zin**    was born in Kedah, Malaysia, in 1987. She received the B.S. degree and M.Sc. degree in Electrical Engineering from Universiti Tun Hussein Onn Malaysia, in 2011 and 2016 respectively. She is currently a Ph.D. student in the School of Electrical Engineering, College of Engineering, Universiti Teknologi MARA, Shah Alam, Malaysia. Since 2016, she has been a lecturer with Universiti Teknologi MARA, Malaysia. Her current research interests include the area of power electronics and motor drives control. She can be contacted at email: adzanie@uitm.edu.my.







**Wan Noraishah Wan Abdul Munim**     received the diploma in Electrical Engineering (telecommunication) from University Teknologi Malaysia, Johor Bahru, Malaysia, in 2003, the B.Eng. Technology degree in Electrical Engineering from Universiti Kuala Lumpur, Kuala Lumpur, Malaysia, in 2007, and the M.Sc. degree In Electrical Power Engineering with business from the University of Strathclyde, Glasgow, U.K., in 2009. Since 2010, she is currently working as a senior lecturer at School of Electrical Engineering, College of Engineering, Universiti Teknologi MARA, Shah Alam, Malaysia. Her research interests include multi-phase machines, fault tolerant control, and renewable energy. Ms. Munim received the 2014 Ministry of Education Malaysia Skim Latihan Akademik IPTA (SLAI) Scholarship Award for her Ph.D. study. She received Ph.D. degrees in Electrical Engineering from the University of Malaya in 2020. She can be contacted at email: aishahmunim@uitm.edu.my.







**Ahmad Farid Abidin**     was born in Malaysia, on Dec 25, 1978. He received his bachelor of engineering in Electrical, Electronic, and System Engineering from Universiti Kebangsaan Malaysia (UKM), M.Sc. in Electrical Engineering from Universiti Teknologi MARA, and Ph.D. degree from Universiti Kebangsaan Malaysia (UKM), in 2000, 2005, and 2011, respectively. He is a professor from Universiti Teknologi MARA, Shah Alam, Malaysia and currently become a top management as a director at the Centre of Foundation Studies, Universiti Teknologi MARA (UiTM), Selangor Branch, Dengkil Campus. His main research interests are in power quality and power system protection. He can be contacted at email: ahmad924@uitm.edu.my.







**Hang Seng Che**     received his B.Eng. degree in Electrical Engineering from the University of Malaya, Malaysia, in 2009. He then obtained his Ph.D. degree in 2013 under auspices of a dual Ph.D. programmer between the University of Malaya and Liverpool John Moores University, Liverpool, UK. He was a senior lecturer in Power Energy Dedicated Advanced Center (UMPEDAC), University of Malaya, Malaysia. Currently, he is the technical director in EV Connection Sdn. Bhd. His research interests are in the areas of electrical machines and drives, power electronics converters for renewable energy conversion, electric vehicles, and charging. He can be contacted at email: hsche@um.edu.my.



**Mohamad Fathi Mohamad Elias**     was born in Sarawak, Malaysia on Oct 30, 1981. He received his B.Eng. (Hons.), M.Eng., and Ph.D. degrees in Electrical Engineering from the University of Malaya, Kuala Lumpur, Malaysia, in 2003, 2007, and 2013, respectively. He is currently a senior lecturer with the Higher Institution Centre of Excellence (HICoE), UM Power Energy Dedicated Advanced Centre (UMPEDAC), Universiti Malaya, Malaysia. His research interests include power electronics, renewable energy, and electrical drives. He can be contacted at email: fathi@um.edu.my.



**Rahimi Baharom**     received his B. Eng. Degree, M.Sc. Degree and Ph.D. from Universiti Teknologi MARA, Malaysia in 2006, 2009 and 2018 respectively. From 2005 to 2009, he was a research assistant at Institute of Research, Development and Commercialization (IRDC) Universiti Teknologi MARA, Malaysia. He is now a senior lecturer at School of Electrical Engineering, College of Engineering, Universiti Teknologi MARA, Malaysia. His research interests include AC-DC converter, wireless power transfer, medium-voltage medium-frequency solid-state transformer, resonant converter with advanced control, and single-phase matrix converter. He can be contacted at email: rahimi6579@uitm.edu.my.